analytical chemistry

pubs.acs.org/ac Article

Multiomics Imaging Using High-Energy Water Gas Cluster Ion Beam Secondary Ion Mass Spectrometry [$(H_2O)_n$-GCIB-SIMS] of Frozen-Hydrated Cells and Tissue

Hua Tian,* Sadia Sheraz née Rabbani, John C. Vickerman, and Nicholas Winograd

Cite This: *Anal. Chem.* 2021, 93, 7808−7814 Read Online

ACCESS | Metrics & More | Article Recommendations | Supporting Information

ABSTRACT: Integration of multiomics at the single-cell level allows the unambiguous dissecting of phenotypic heterogeneity at different states such as health, disease, and biomedical response. Imaging mass spectrometry holds the promise of being able to measure multiple types of biomolecules in parallel in the same cell. We have explored the possibility of using water gas cluster ion beam secondary ion mass spectrometry [$(H_2O)_n$-GCIB-SIMS] as an analytical tool for multiomics assay. $(H_2O)_n$-GCIB has been hailed as an ideal ionization source for biological sampling owing to the enhanced chemical sensitivity and reduced matrix effect. Taking advantage of 1 μm spatial resolution by using a high-energy beam system, we have clearly shown the enhancement of multiple intact biomolecules up to a few hundredfold in single cells. Coupled with the cryogenic sample preparation/measurement, the lipids and metabolites were imaged simultaneously within the cellular region, uncovering the pristine chemistry for integrated omics in the same sample. We have demonstrated that double-charged myelin protein fragments and single-charged multiple lipids and metabolites can be localized in the same cells/tissue with a single acquisition. Our exploration has also been extended to the capability of $(H_2O)_n$-GCIB in the generation of multiple charged peptides on protein standards. Frozen hydration combined with $(H_2O)_n$-GCIB provides the possibility of universal enhancement for the ionization of multiple bio-molecules, including peptides/proteins which has allowed "omics" to become feasible in the same sample using SIMS.

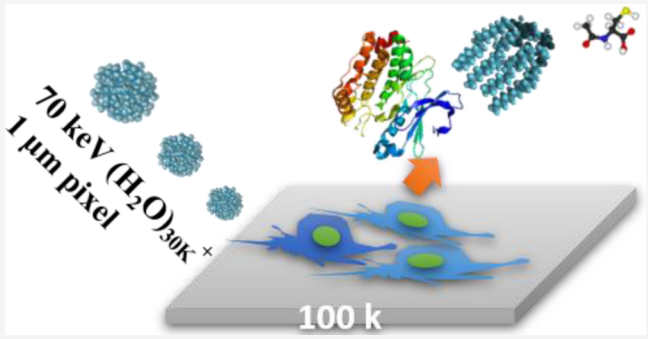

INTRODUCTION

Interpretation of interaction and variations of biomolecules at the level of multiomics allows a comprehensive understanding of healthy and diseased biological systems. Multiomics is a platform used to describe integration of data sets from all different types of "omics" such as genome, transcriptome proteome, lipidome, and metabolome, which in turn has made significant contributions to the characterization of complex biological systems, providing an insight into the mechanism of various diseases and the development of therapeutic strategies.[1,2] Biologists are increasingly interested in single-cell "omics", which provides a complete spectrum of biomolecules that are not confounded by the heterogeneity of bulk samples, thus enabling insights to be gained into cellular phenotype, heterogeneity, and response to treatment.[3−5]

To engage any level of single-cell omics, a crucial step is to isolate single cells from the tissue to a format that can be processed for the different downstream mono-omics. With the advance of isolation techniques combined with compatible detection approaches, it is now possible for multiomics studies to be carried out on the same cell. For example, simultaneous detection of DNA and RNA or RNA and protein.[2] In spite of remarkable achievements, the metabolomic and lipidomic approaches mainly rely on the assay of the bulk extracts of cells and tissues using liquid chromatography mass spectrometry (LC/MS).[6] These approaches take the single cells out of their complex biomatrices and provide no spatial information of important biomolecules; however, cellular/subcellular localization of these biomolecules is vital for further understanding of the biological and physiological processes taking place. This approach is even more problematic for metabolic studies in single cells owing to the fast changes and dynamic nature of the processes and the difficulty for preservation in time and space. Moreover, there are no available tags to amplify and register the small metabolites of interest, the approach conventionally used for proteins. MS imaging (MSI) has opened a new era for the multiomics study because of the capability to spatially localize multiple molecular species in a

Received: December 12, 2020
Accepted: April 5, 2021
Published: May 26, 2021

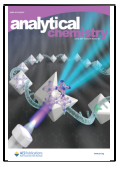

single run with minimum sample preparation and without tags.[7,8] Matrix-assisted laser desorption/ionization (MALDI), one of the widely used MSI system, alone can be used to study different "omics". The technique advances in MALDI have allowed subcellular imaging at the resolution of a few microns for single-cell omics.[9−12] Considering the chemical sensitivity and sample preparation associated with matrix application, it remains a challenge to uncover the pristine chemistry in single cells using MALDI. The other MSI tools, such as laser ablation electrospray ionization MS,[13] nanospray desorption electrospray ionization,[14] liquid extraction surface analysis (LESA),[15] nanodroplet processing in one pot for trace samples with laser microdissection,[16] and multiplexed ion beam imaging,[17] have also been employed for spatial omics. However, integrating different spatial omics at the single-cell level still remains ineffective using a single tool or workflow either due to the incompatibility of the sample preparation or the lack of spatial resolution.

Among the contemporary MSI tools, gas cluster ion beam secondary ion MS (GCIB-SIMS) has been developed for molecular mapping to localize multiple biomolecules, particularly intact lipids with reasonable spatial resolution.[18,19] Argon GCIB (Ar-GCIB) was first introduced by the Kyoto group of Yamada and Matsuo, and initially, it was used as a sputtering source to clean the surfaces and to remove the chemical damage caused by highly focused atomic ion beams.[20,21] However, the advantages of low chemical damage and intact molecule detection were swiftly recognized by the SIMS community and hence was employed as a primary ion source for many applications.[22] Although Ar-GCIB gained quite a momentum in recent years, the low spatial resolution due to technical difficulties and low ionization efficiency were still a cause of concern.

Various strategies have been developed to tackle these challenges in the applications of GCIB. Our approach of chemical doping of Ar cluster (CH_4/HCl/CO_2 mixed Ar cluster beam) has demonstrated the enhanced ionization and alternative gas candidates $(CO_2)_n$-GCIB for better focus.[23−25] Other researchers have also been trying to maximize the potential of the GCIB. For example, Fletcher et al., has adopted high energy (∼40 keV) Ar cluster ion beams to generate 3 μm focused beam to image various biological systems where large biomolecules, such as gangliosides and intact phospholipids, were mapped.[18] 2−3 μm resolution of GCIB has also been shown by Matsuo and Gilmore.[18,19,22] The Vickerman and Lockyer group has been focusing on the development of water cluster ion beams and enhancement of up to ∼100-fold has been reported on various biomolecules. The imaging capability of water beams has also been explored at a lower resolution ∼20−50 μm.[26] It was not possible to image subcellular structures at ∼1 μm resolution using GCIB until the introduction of ∼70 keV $(CO_2)_n$-GCIB.[27] In collaboration with Vickerman, ∼70 keV H_2O cluster beams were successfully explored, taking full advantage of the high-spatial resolution and high ionization. Focused down to a ∼1 μm spot, a 70 keV $(H_2O)_n$-GCIB has enhanced intact biomolecules [e.g., phospholipids, cardiolipins (CL), and gangliosides] by up to a few hundredfold on frozen-hydrated HeLa cells.[28] This achievement has allowed for the imaging of lipids at low concentrations, particularly, oxidized CL and phosphoethanolamine (PE) at the subcellular level and this has laid the ground for characterization and localization of additional biomolecules with the ultimate aim to determine its application in "multiomics".

Here, we explore the potential of GCIB-SIMS, particularly with the further development of a 70 keV water cluster ion beam to integrate multiomics imaging in the same samples (cell and tissue) and under similar sample preparation conditions. We have also validated the sample preparation, frozen hydration where cryo-preservation and cryogenic analysis preserve the cellular contents in time and space without diffusion and delocalization. Among four common methods that are currently used, chemical fixation, freeze-fracturing, frozen hydration, and freeze-drying, frozen hydration is believed to be the most successful in preserving the integrity of biological specimen as well as increasing ionization, but it is technically the most challenging of all.[29−31] Taking advantage of subcellular resolution and enhanced ionization of $(H_2O)_n$-GCIB and cryogenic analysis, we have demonstrated that double-charged protein fragments and single-charged multiple lipids and metabolites can be localized in the same cells/tissue with a single acquisition. In contrast, chemically fixed cells showed delocalized metabolites outside the cellular regions. Further, investigation of the generation of multi-charged peptides/protein standards has also been conducted. This study has shown the potential of $(H_2O)_n$-GCIB-SIMS for spatial multiomics assay in frozen-hydrated biosamples, especially for single-cell metabolomics which presents challenges for sample preservation and spatial localization in individual cells.

MATERIALS AND METHODS

Cell Preparation. The standard procedure was used to culture HeLa cells in Dulbecco's modified Eagle medium (Corning, US) media in an incubator at 37 °C with 5% CO_2. Upon the confluence of 60%, the cells were passaged to 6-well plates placed with pre-cleaned silicon wafers (5 × 5 mm^2, sonicated in chloroform, water, and methanol for 5 min each, respectively). After overnight growth (12 h), the wafers were washed with 0.15 M ammonium formate (≥99.0%, Sigma, Milwaukee, US) solution swiftly three times. Three wafers were then fixed with 2% glutaraldehyde (GA, Sigma, Milwaukee, US) for 15 min, then air-dried, and another three wafers were plunge-frozen in liquid ethane and then mounted onto a liquid nitrogen (LN_2)-cooled sample holder.

Animal Tissue Preparation. The coronal section of the mouse brain was sliced at 5 μm at −20 °C using a cryostat (Leica CM1950). The two serial sections were received onto indium tin oxide glass plate and then frozen by plunging into LN_2, followed by mounting onto a sample stub under LN_2.

Peptide/Protein Standards Preparation. A melittin standard [≥97% (HPLC), Sigma, Milwaukee, US], a large peptide consisting of 26 amino acids, was prepared using two different methods, one in water and the second in a mixed solvent S1 [H_2O/acetonitrile (ACN)/formic acid = 59:40.5:0.5] at a concentration of 2.5 mg/mL. 0.1 μL of the solution was dropped onto the pre-cleaned Si wafer to form a thin aqueous film and then plunged into LN_2. To investigate the multiple charging enhancers, melittin and human insulin (BioReagent, Sigma, Milwaukee, US) were prepared with mixed solvents S2 (solvent 1/HCl = 99:1) and S3 [5 mg 3-nitrobenzonitrile (3-NBN) in 100 μL 50% ACN] at a concentration of 2.5 mg/mL. 0.1 μL of the solutions was used to prepare the thin ice-films using the same procedure.

https://doi.org/10.1021/acs.analchem.0c05210
Anal. Chem. 2021, 93, 7808−7814

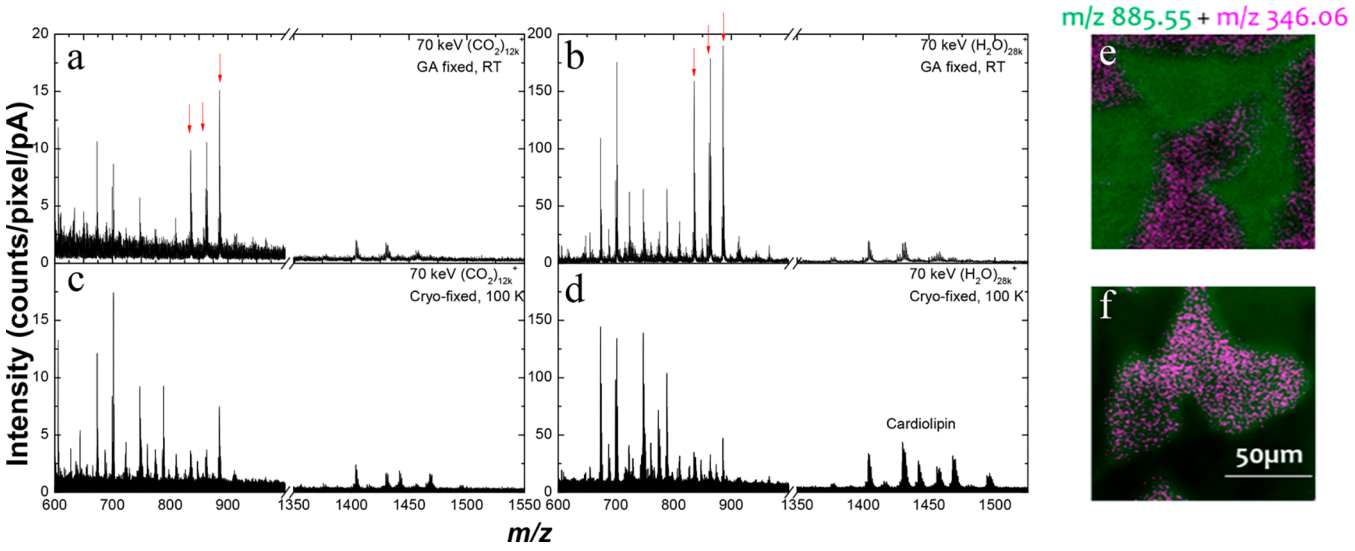

Figure 1. Negative spectra from the cell samples, surface and color overlay images of HeLa cells. Cell surface spectra were acquired at different conditions (a) GA fixed, RT using 70 keV $(CO_2)_{12k}^+$; (b) GA fixed, RT using 70 keV $(H_2O)_{28k}^+$; (c) frozen-hydrated, 110 K using 70 keV $(CO_2)_{12k}^+$; (d) frozen-hydrated, 110 K using 70 keV $(H_2O)_{28k}^+$. Lipids at m/z 835.50, 863.53, and 885.55 become the dominant signals from cell surface as the red arrows point in (a) and (b), indicating that chemical fixation could induce further chemical changes or lipid migration to the sample surface. Color overlay images show the distribution of PI (38:4) at m/z 885.55 in green and AMP at m/z 346.06 in magenta using 70 keV $(H_2O)_{28k}$ at different sample preparations, (e) GA fixed, RT; and (f) frozen-hydrated, 110 K.

The samples were placed onto the pre-cooled sample holder under LN_2.

To determine the detection limit of melittin, 1 mM (2.8 mg/mL) of melittin was diluted with water for the final concentrations of 1, 1×10^{-1}, 1×10^{-2}, 1×10^{-3}, 1×10^{-4}, 1×10^{-5}, and 1×10^{-6} mM. 90 μL of each solution was spin-coated onto pre-cleaned gold-coated silicon wafers using a spin coater (Laurell Technologies, Model WS 650-MZ, North Wales, PA, US) at 5000 rpm. The silicon wafers with the thin melittin film were immediately submerged into LN_2 followed by mounting onto the sample holder under LN_2.

With the purging of dry N_2, the cold sample holder with the samples mentioned above was inserted into the pre-cooled sample stage for cryogenic SIMS measurement.

SIMS Measurement. A DC beam buncher-ToF instrument, J105 3D Chemical Imager (Ionoptika Ltd., UK) was used for SIMS imaging and analysis.[32] The system is equipped with a unique 70 keV GCIB with the capability of generating a giant water cluster beam. A cryogenic sample handling facility enables the analysis of biological samples in a frozen-hydrated state.

Two different cell samples were imaged using 70 keV $(CO_2)_{11,500}^+$ and 70 keV $(H_2O)_{28,000}^+$ beams at a spot size of 1 μm over an area of 128×128 μm^2 with 128×128 pixels at a beam dose of 5.63×10^{12} ions·cm^{-2}. This scan was continued until the cellular material was consumed, the so-called 3D-depth profiling.

For tissue imaging, the 70 keV $(H_2O)_{31,000}^+$ beam was focused to 6 μm to scan an area of 2.94×3.78 mm^2 in the cerebellum region of mouse brain tissue by stitching 7×9 tile images together. Each tile was scanned with 64×64 pixels at the water beam dose of 2.88×10^{11} ions·cm^{-2}.

The surface spectra were acquired from peptide standards using 70 keV pure $(H_2O)_{28,000}^+$ and 70 keV pure $(CO_2)_{11,500}^+$. Three parallel analyses were performed to acquire the spectra with an ion dose of 2.21×10^{12} ions·cm^{-2}.

Data Processing. Ionoptika analyser (2.0.2.11) was used to generate the images of the ions of interest, color overlay images, and ion intensity readout. All the images were generated by selecting the mass window of $\Delta m = 0.02$ around the centroid mass. The contrast level and the maximum signal counts beside the images were shown on the gray scale bar. The molecular ion intensity of melittin at different concentrations was summed by the ions of m/z 2846.41, 2847.43, 2848.43, and 2849.43 with a mass width of $\Delta m = 0.9$, respectively.

RESULTS AND DISCUSSION

Frozen Hydration Is the Key for Imaging of Single-Cell Omics. Frozen-hydrated analysis has been proven to be an optimal method to preserve the biological sample as close as possible to their native state for MSI imaging.[29,33−36] This requires the ultra-rapid freezing of the biosamples in liquid nitrogen/ethane/propane and the maintenance the cryogenic temperature (100 K) during the entire sample transfer and measurement. Previous studies have demonstrated the migration of lipids and changes on the tissues with varying sample preparations, mainly non-frozen hydration versus frozen hydration.[30,36−38] However, the small diffusible metabolites in single cells have not been compared previously with different sample preparations. Here, we mainly focus on how the metabolites change with the widely used sample preparations for single-cell MSI, chemical fixation, and frozen hydration.[31,35] We first validated the frozen-hydrated sample preparation using CryoSEM. Figure S1 shows CryoSEM images of HeLa cells cultured on the Si wafer and prepared by plunging into liquid ethane and liquid nitrogen. The images at 276×, 455×, and 848× show that the cells have been preserved properly without lysis or bursting. The cellular morphology and sizes are consistent with the microscopy images reported previously.[39]

The cell imaging was performed to investigate the biological information in terms of the signal level and distribution using

https://doi.org/10.1021/acs.analchem.0c05210
Anal. Chem. 2021, 93, 7808−7814

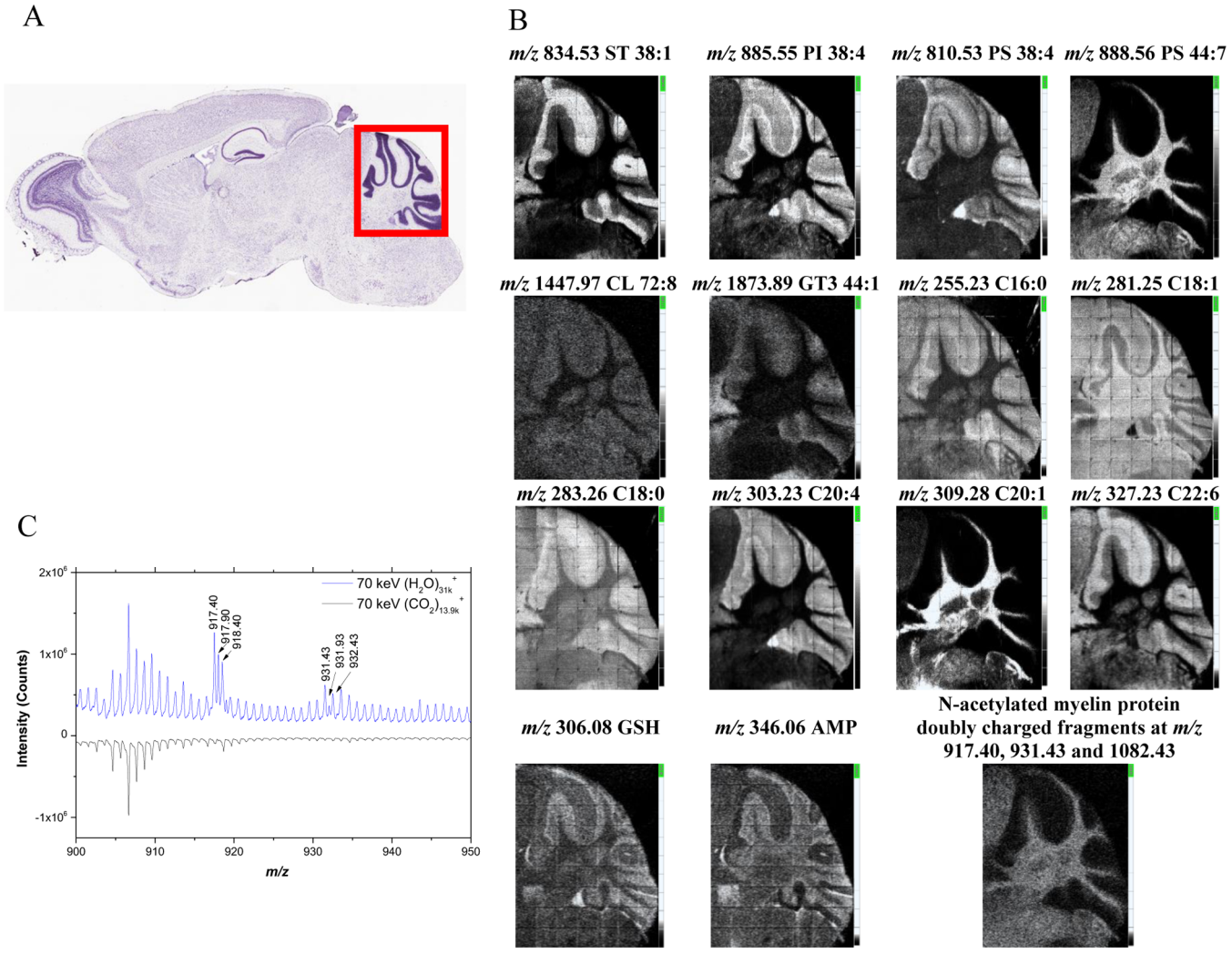

Figure 2. Simultaneous imaging of metabolites, lipids, and protein fragments on mouse brain tissue using 70 keV $(H_2O)_{31k}^+$. (A) H&E staining image of mouse brain tissue. The area of 2.94 × 3.78 mm^2 highlighted in red was imaged using 70 keV $(H_2O)_{31k}^+$ at a pixel size of 6 μm; (B) Single-ion images of selected ions. Lipid abbreviations: ST, sulfatide; PI, phosphatidylinositol; PE, phosphatidylethanolamine; PS, phosphatidylserine; CL, cardiolipin; and AMP, adenosine monophosphate; (C) Mass spectrum of the mouse brain tissue shows the doubly charged ions at m/z 917.40, 917.90, 918.40, 931.43, 931.93, and 932.43 using 70 keV $(H_2O)_{31k}^+$. These ions are not observed using 70 keV $(CO_2)_{13.5k}^+$. More details are shown in the full spectrum in Figure S3.

H_2O and CO_2 cluster beams with varying sample preparations. From the surface spectra in Figure 1, it is clear that (1) the water beam enhances the intact lipid signals regardless of the sample preparation as seen in Figure 1b,d in comparison with Figure 1a,c, particularly for low abundance lipids, such as phosphatidic acid (m/z 773.52), phosphatidylserine (PS, m/z 760.53 and 847.42), and CLs (m/z 1400−1500), where a ∼200-fold increase in signal is noticed, Table S1. This enhancement can be attributed to the deprotonation by negative OH^- which is released upon the impact of the water beam. (2) The GA fixed samples show the lipid migration regardless of the beam type. Lipids at m/z 835.50, 863.53, and 885.55 become the dominant signals as red arrows point in Figure 1a,b, indicating that chemical fixation could induce further chemical changes or lipid migration to the sample surface. (3) More importantly, the delocalization of metabolites is observed in the GA fixed cells with the subcellular imaging at a spatial resolution of ∼1 μm, as shown in Figure 1e, wherein, small metabolite, adenosine monophosphate (AMP), at m/z 346.06 in magenta is localized outside of the cellular region, represented by the membrane lipid phosphatidylinositol (PI) (38:6) at m/z 885.55 in green. In contrast, the cell image in the frozen-hydrated state, the most native-state of the bio-system, shows that AMP is co-localized within PI (38:6), Figure 1f. The localization of a wide range of small metabolites such as adenosine triphosphate, glutathione (GSH), glucose, and so forth, show the same phenomenon in chemically fixed and frozen-hydrated cells as seen in Figure S2. The empirical assignment of the ions can be referred to in Table S2.

With the signal enhancement by the water cluster beam, it will benefit the localization of low abundance biomolecules in its protonated or deprotonated form. However, special attention must be paid to sample preparation. To capture the native state of the cellular chemistry, especially for the dynamic and fast-moving metabolites, frozen hydration is the only optimal sample preparation to enable image capture of the complex cellular chemistry at high-spatial resolution. The majority of the previous studies on the cellular metabolites were based on the chemically fixed and overly prepared cells, in

https://doi.org/10.1021/acs.analchem.0c05210
Anal. Chem. 2021, 93, 7808−7814

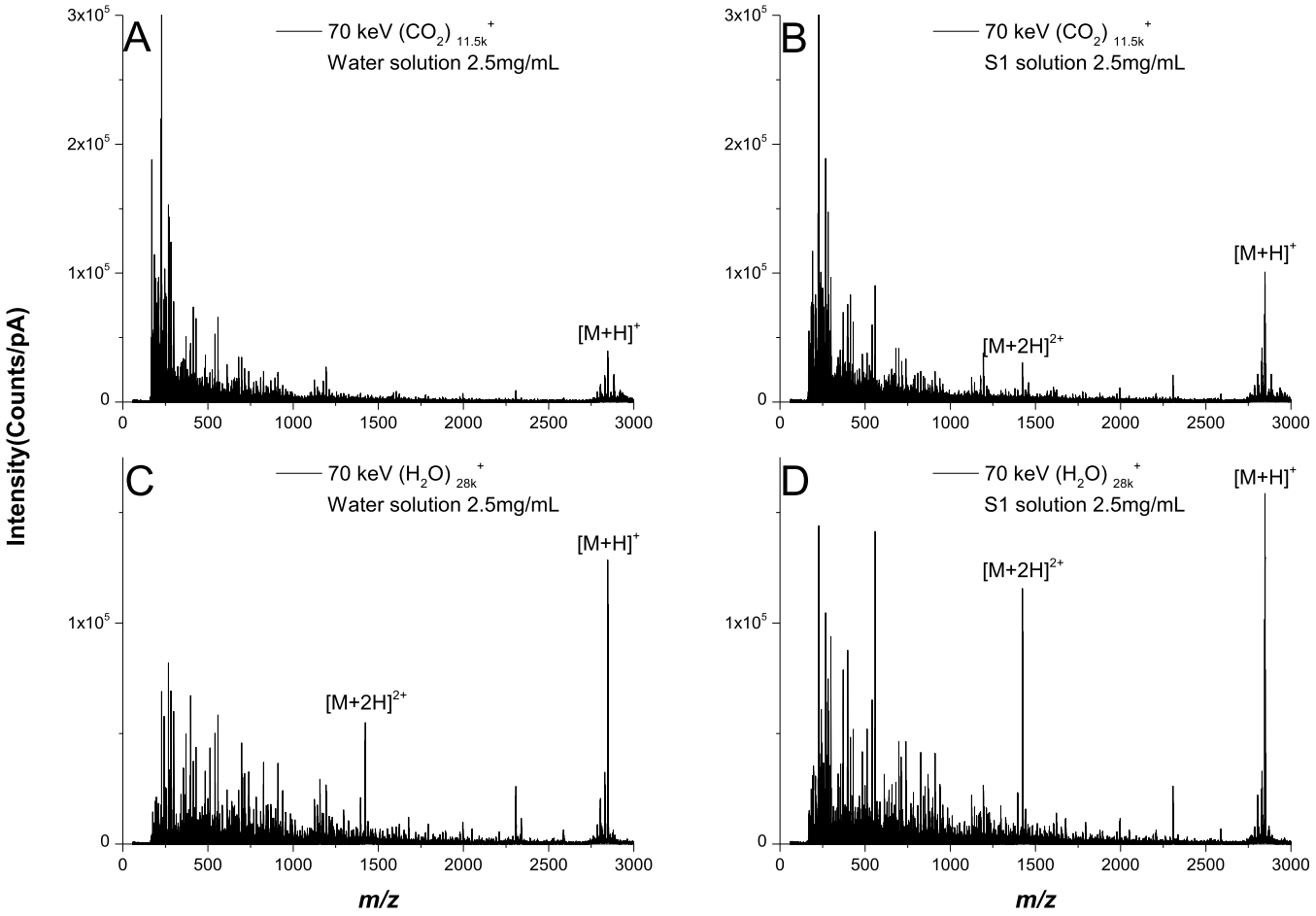

Figure 3. Positive spectra of melittin acquired at −100 K under different conditions, (A) spin-coated film using 70 keV $(CO_2)_{11.5k}^+$; (B) ice-film using 70 keV $(CO_2)_{11.5k}^+$; (C) spin-coated film using 70 keV $(H_2O)_{28k}^+$; and (D) ice-film using 70 keV $(H_2O)_{28k}^+$. Water beam at condition D not only enhances $[M + H]^+$ by 1.5 times but also $[M + 2H]^{2+}$ by three times compared with condition B. At condition C, water beam enhances $[M + H]^+$ by three times and $[M + 2H]^{2+}$ infinitely as compared with condition A.

which, the subcellular distribution was lost long before the analysis.

This approach serves as a complementary tool to provide the information on multiple small phenotypically relevant biomolecules that are not distinguishable due to the blurring of compositional heterogeneity implicit in conventional bulk assays. Rather than an assay of millions of cells, the workflow focuses on the spatial correlation of the intermediates and end products of the biosynthesis, offering a direct visualization of functional metabolite pathways channeled through relevant protein complexes. Without the sufficient MS/MS capability, the GCIB-SIMS will have to be complemented by parallel LC/MS and isotopic labeling to confirm the identities of the metabolites. Therefore, untargeted metabolite profiling using the current instrument setting has limited applications in complex biosystems.

Multiomics Imaging on Frozen Tissue. The signal enhancement was also observed on a tissue sample using 70 keV $(H_2O)_{31k}^+$ which falls into the optimum energy range of 0.13−0.20 eV/nucleon.[28,40] The cerebellum region on mouse brain tissue was imaged with a defocused water cluster ion beam, 6 μm/pixel to reduce the acquisition time and data redundancy.

The analyzed cerebellum region is highlighted in the H&E image in Figure 2A. Figure 2B shows selected ion maps, especially some low-intensity species that can be localized to different anatomical layers. All the observed ions are listed in Table S2. For example, sulfatide (ST) 38:1 at m/z 834.58 and fatty acid (FA) C22:6 at m/z 327.23 are concentrated in the outer layer of the cerebellum cortex, molecular layer. FA C18:0 at m/z 283.26 is also elevated in this layer; PI 38:4 at m/z 885.55 and FA C20:4 at m/z 303.23 are elevated in the middle layer, Purkinje layer; PS 38:4 at m/z 810.53 and FA C20:4 at m/z 303.23 are localized in both the outer molecular and inner granular layers; PS 44:7 at m/z 888.53 and FA C 20:1 at m/z 309.27 are specially localized in the white matter. We also observed other low-intensity species, such as CL (72:8) at m/z 1447.97 in all the layers and ganglioside GT3 44:1 at m/z 1873.89 in the molecular layer. The low-intensity species (e.g., PS, CL, and gangliosides) can be localized due to the signal enhancement for deprotonated molecular species $[M - H]^-$. Using other desorption sources (i.e., Ar cluster and CO_2 cluster), these species were either invisible or detected at such a low intensity that might not be sufficient for imaging.

The small metabolites were also localized simultaneously since the dynamic chemical flux was preserved by the cryogenic sample preparation and analysis. GSH m/z 306.08 and AMP at m/z 346.05 show very distinct localizations in the granular layer and granular layer plus white matter, respectively. Most interestingly, the multi-charged ions are observed as shown in the spectrum in Figures 2C and S3 using 70 keV $(H_2O)_{31k}^+$. The difference of Δ m/z 0.5 between ions

https://doi.org/10.1021/acs.analchem.0c05210
Anal. Chem. 2021, 93, 7808−7814

at m/z 917.40, 917.90, and 918.40 indicates that these are doubly charged ions. The half-mass intervals are also seen in triplet ions at m/z 931.43, 931.93, and 932.43, and at m/z 1082.43, 1082.93, and 1082.43. These doubly charged ions are not observed in the same area on a serial section using 70 keV $(CO_2)_{13.5k}^+$. A literature search shows that all the doubly charged ions match the fragments of N-acetylated myelin protein.[41] However, further identification is not possible with the current MS/MS capability of the instrument. All these ions are mapped on the tissue with elevated intensity in the white matter (Figure 2B).

For the first time, we have shown the capability of simultaneous imaging of metabolites, lipids, and protein fragments in a single sample and single acquisition. With the cryogenic sample handling system, the tissue was analyzed in frozen-hydrated state at 100 K, the gold standard to maintain the biological sample in the close-to-nature state. Therefore, the original chemical gradients of multiomics are mapped in time and space, leading to a comprehensive picture of biological events and network connections at near-nature states. Moreover, the water contained in the tissue is likely to enhance the proton transfer for the generation of multiple charged protein ions, and the further investigation of possible enhancers is described in the following section.

Possibility of Protein/Peptide Detection. The capability of protein/peptide detection was further demonstrated through standard analysis. Melittin, consisting of 26 amino acids was analyzed in two different sample preparations, first in water and second in an ice matrix of S1 (H_2O/ACN/formic acid = 59:40.5:0.5 by volume). Solvent S1 is used in LESA imaging[42] to extract the protein directly from the frozen-hydrated biological sample surface, benefiting from the effect of protein structure unfolding and multiple ionization. In positive ion mode, the yields of $[M + H]^+$ is enhanced by threefold, and infinitely for $[M + 2H]^{2+}$ from the ice-film of melittin water solution using 70 keV $(H_2O)_{28k}^+$ (Figure 3C) compared to using 70 keV $(CO_2)_{11.5k}^+$ with the same energy of 0.13 eV/nucleon (Figure 3A). The enhancement for $[M + H]^+$ and $[M + 2H]^{2+}$ is further boosted from the ice-film of melittin S1 solution (Figure 3D), by 1.2- and 2.2-fold compared with condition C using 70 keV $(H_2O)_{28k}^+$ (Figure 3C), while it is 1.5- and 3-fold compared with condition B using 70 keV $(CO_2)_{11.5k}^+$ (Figure 3B).

The possibility of enhancing the doubly charged ion and higher charge states was also investigated using only water cluster ion beam on melittin and insulin films with the different enhancers. As shown in Figure S4, compared with pure water ice-film of two peptides (Figure S4A,B), S1 solution plus 1% HCl ice-film enhances $[M + 2H]^{2+}$ by 5−10-fold (Figure S4C,D). The higher charge states, $[M + 3H]^{3+}$ and $[M + 4H]^{4+}$ are promoted in 3-NBN and ACN ice-film for both peptides (Figure S4E,F). It is clearly seen that the ice matrices with strong acidification and polarization benefit the formation of multiple charged molecular ions under the bombardment of the water cluster beam. The peptide usually does not favor the negative ionization. However, the water cluster beam can still enhance $[M - H]^-$ by two times compared with a $(CO_2)_n$-GCIB from the ice-film of melittin S1 solution (Figure S5B,D) and 4.5 times compared with $(CO_2)_n$-GCIB from the ice film of melittin water solution (Figure S5A,D. Lastly, from a plot of the intensity of molecular ion $[M + H]^+$ as a function of concentration (Figure S6), the detection limit of melittin is determined to be approximately 10 μM (0.028 mg/mL) using 70 keV $(H_2O)_{28k}^+$. With the wide concentration range of peptides in biological systems, particularly their aggregation in certain diseases reaching up to the level of mM,[43] there is the potential of using the water cluster beam to map their localizations at high-spatial resolution.

Generating multiple charged ions using the water cluster ion beam brings down the mass detection range of large peptides and proteins, providing an opportunity to simultaneously acquire a wider range of biomolecules, (e.g., metabolites, lipids, and protein/peptides). However, the lower concentration of protein/peptides than lipids in the tissue/cells could hinder the direct imaging of these species without the enhancers (i.e., formic acid, HCl, and 3-NBN). Tuning the beam chemistry with the protein enhancers could be a solution and will be explored in the future work.

CONCLUSIONS AND OUTLOOK

Combining the $(H_2O)_n$-GCIB-SIMS and cryogenic sample handling, we have demonstrated the possibility to integrate multiomics imaging in the same biological sample at near-nature state. The desorption source determines the spatial resolution and chemical sensitivity. We have shown that the water cluster ion beam operating at a high energy of ∼70 keV is able to achieve the spatial resolution at 1 μm without compromising the chemical sensitivity, which usually are incompatible properties with the other desorption sources. Especially, the water cluster ion beam enhances the low-intensity lipids and metabolites in the biological samples, making it possible to image these species at the single-cell level. We also demonstrated a valid sample preparation, frozen hydration to immobilize all the analytes in time and space, avoiding the migration or delocalization of the biomolecules particularly for the dynamic metabolites at subcellular level. With this setup, the imaging of peptide and protein fragments at a high-spatial resolution became possible along with the smaller molecules, metabolites, and lipids, in the same sample and with a single acquisition using 70 keV $(H_2O)_n$-GCIB-SIMS, the former benefiting from the generation of multiple charged ions. The established methodology opens a new opportunity for the single-cell multiomics imaging for an unambiguous interpretation of cell heterogeneity in different states such as healthy, diseased, and in response to biomedical treatment. Tuning the beam chemistry and adapting the lanthanide-tagged antibodies for enhanced proteins imaging will also be explored and reported in future studies.

ASSOCIATED CONTENT

Supporting Information

The Supporting Information is available free of charge at https://pubs.acs.org/doi/10.1021/acs.analchem.0c05210.

Signal enhancement of selected species using water cluster ion beam in comparison with CO_2 cluster ion beam; empirical assignment of the ion species discussed in the study; validation of HeLa cell sample preparation using CryoSEM; distribution of various small metabolites in frozen-hydrated cell versus chemically fixed cell; and further experimental results on peptide/protein analysis using water cluster ion beam coupled with the enhancer and detection limit (PDF)

https://doi.org/10.1021/acs.analchem.0c05210
Anal. Chem. 2021, 93, 7808−7814

AUTHOR INFORMATION

Corresponding Author

Hua Tian − *Department of Chemistry, Pennsylvania State University, University Park, Pennsylvania 16802, United States;* orcid.org/0000-0002-3598-0219; Email: hut3@psu.edu

Authors

Sadia Sheraz née Rabbani − *The Rosalind Franklin Institute, Didcot OX11 0FA, U.K.*

John C. Vickerman − *Manchester Institute of Biotechnology, University of Manchester, Manchester M1 7DN, U.K.*

Nicholas Winograd − *Department of Chemistry, Pennsylvania State University, University Park, Pennsylvania 16802, United States*

Complete contact information is available at: https://pubs.acs.org/10.1021/acs.analchem.0c05210

Author Contributions

H.T. conceived the project and drafted the initial manuscript. S.S.n.R. and J.C.V. compiled and edited the manuscript and provided critique. N.W. provided critique.

Notes

The authors declare no competing financial interest.

ACKNOWLEDGMENTS

We would like to acknowledge funding from National Institute of Health (NIH) grant number: 1UG3CA256962-01.

REFERENCES

(1) Subramanian, I.; Verma, S.; Kumar, S.; Jere, A.; Anamika, K. *Bioinf. Biol. Insights* **2020**, *14*, 117793221989905.

(2) O'Donnell, S. T.; Ross, R. P.; Stanton, C. *Front. Microbiol.* **2020**, *10*, 3084.

(3) Peng, A.; Mao, X.; Zhong, J.; Fan, S.; Hu, Y. *Proteomics* **2020**, *20*, 1900271.

(4) Nam, A. S.; Chaligne, R.; Landau, D. A. *Nat. Rev. Genet.* **2020**, *22*, 3−18.

(5) Lee, J.; Hyeon, D. Y.; Hwang, D. *Exp. Mol. Med.* **2020**, *52*, 1428−1442.

(6) González-Riano, C.; Dudzik, D.; Garcia, A.; Gil-de-la-Fuente, A.; Gradillas, A.; Godzien, J.; López-Gonzálvez, Á.; Rey-Stolle, F.; Rojo, D.; Ruperez, F. J.; Saiz, J.; Barbas, C. *Anal. Chem.* **2020**, *92*, 203−226.

(7) Xu, G.; Li, J. *J. Comp. Neurol.* **2019**, *527*, 2158−2169.

(8) Quanico, J.; Franck, J.; Wisztorski, M.; Salzet, M.; Fournier, I. *Biochim. Biophys. Acta, Gen. Subj.* **2017**, *1861*, 1702−1714.

(9) Zavalin, A.; Todd, E. M.; Rawhouser, P. D.; Yang, J.; Norris, J. L.; Caprioli, R. M. *J. Mass Spectrom.* **2012**, *47*, 1473−1481.

(10) Zavalin, A.; Yang, J.; Hayden, K.; Vestal, M.; Caprioli, R. M. *Anal. Bioanal. Chem.* **2015**, *407*, 2337−2342.

(11) Kompauer, M.; Heiles, S.; Spengler, B. *Nat. Methods* **2017**, *14*, 90−96.

(12) Rubakhin, S. S.; Greenough, W. T.; Sweedler, J. V. *Anal. Chem.* **2003**, *75*, 5374−5380.

(13) Etalo, D. W.; Díez-Simón, C.; de Vos, R. C. H.; Hall, R. D. Laser Ablation Electrospray Ionization-Mass Spectrometry Imaging (LAESI-MS) for Spatially Resolved Plant Metabolomics. In *Plant Metabolomics: Methods and Protocols*; António, C., Ed.; Springer New York: New York, NY, 2018; pp 253−267.

(14) Yin, R.; Burnum-Johnson, K. E.; Sun, X.; Dey, S. K.; Laskin, J. *Nat. Protoc.* **2019**, *14*, 3445−3470.

(15) Sarsby, J.; Griffiths, R. L.; Race, A. M.; Bunch, J.; Randall, E. C.; Creese, A. J.; Cooper, H. J. *Anal. Chem.* **2015**, *87*, 6794−6800.

(16) Zhu, Y.; Piehowski, P. D.; Zhao, R.; Chen, J.; Shen, Y.; Moore, R. J.; Shukla, A. K.; Petyuk, V. A.; Campbell-Thompson, M.; Mathews, C. E.; Smith, R. D.; Qian, W.-J.; Kelly, R. T. *Nat. Commun.* **2018**, *9*, 882.

(17) Keren, L.; Bosse, M.; Marquez, D.; Angoshtari, R.; Jain, S.; Varma, S.; Yang, S.-R.; Kurian, A.; Van Valen, D.; West, R.; Bendall, S. C.; Angelo, M. *Cell* **2018**, *174*, 1373−1387.

(18) Angerer, T. B.; Blenkinsopp, P.; Fletcher, J. S. *Int. J. Mass Spectrom.* **2015**, *377*, 591−598.

(19) Passarelli, M. K.; Pirkl, A.; Moellers, R.; Grinfeld, D.; Kollmer, F.; Havelund, R.; Newman, C. F.; Marshall, P. S.; Arlinghaus, H.; Alexander, M. R.; West, A.; Horning, S.; Niehuis, E.; Makarov, A.; Dollery, C. T.; Gilmore, I. S. *Nat. Methods* **2017**, *14*, 1175−1183.

(20) Toyoda, N.; Matsuo, J.; Aoki, T.; Yamada, I.; Fenner, D. B. *Nucl. Instrum. Methods Phys. Res., Sect. B* **2002**, *190*, 860−864.

(21) Ninomiya, S.; Ichiki, K.; Yamada, H.; Nakata, Y.; Seki, T.; Aoki, T.; Matsuo, J. *Rapid Commun. Mass Spectrom.* **2009**, *23*, 1601−1606.

(22) Matsuo, J.; Torii, S.; Yamauchi, K.; Wakamoto, K.; Kusakari, M.; Nakagawa, S.; Fujii, M.; Aoki, T.; Seki, T. *Appl. Phys. Express* **2014**, *7*, 056602.

(23) Wucher, A.; Tian, H.; Winograd, N. *Rapid Commun. Mass Spectrom.* **2014**, *28*, 396−400.

(24) Tian, H.; Wucher, A.; Winograd, N. *J. Am. Soc. Mass Spectrom.* **2016**, *27*, 285−292.

(25) Tian, H.; Maciążek, D.; Postawa, Z.; Garrison, B. J.; Winograd, N. *J. Am. Soc. Mass Spectrom.* **2016**, *27*, 1476−1482.

(26) Sheraz née Rabbani, S.; Berrueta Razo, I.; Kohn, T.; Lockyer, N. P.; Vickerman, J. C. *Anal. Chem.* **2015**, *87*, 2367−2374.

(27) Tian, H.; Sparvero, L. J.; Blenkinsopp, P.; Amoscato, A. A.; Watkins, S. C.; Bayır, H.; Kagan, V. E.; Winograd, N. *Angew. Chem., Int. Ed. Engl.* **2019**, *131*, 3188−3193.

(28) Sheraz, S.; Tian, H.; Vickerman, J. C.; Blenkinsopp, P.; Winograd, N.; Cumpson, P. *Anal. Chem.* **2019**, *91*, 9058−9068.

(29) Henss, A.; Hild, A.; Rohnke, M.; Wenisch, S.; Janek, J. *Biointerphases* **2015**, *11*, 02A302.

(30) Malm, J.; Giannaras, D.; Riehle, M. O.; Gadegaard, N.; Sjövall, P. *Anal. Chem.* **2009**, *81*, 7197−7205.

(31) Robinson, M. A.; Castner, D. G. *Biointerphases* **2013**, *8*, 15.

(32) Fletcher, J. S.; Rabbani, S.; Henderson, A.; Blenkinsopp, P.; Thompson, S. P.; Lockyer, N. P.; Vickerman, J. C. *Anal. Chem.* **2008**, *80*, 9058−9064.

(33) Chandra, S.; Morrison, G. H. *Biol. Cell* **1992**, *74*, 31−42.

(34) Piwowar, A. M.; Fletcher, J. S.; Kordys, J.; Lockyer, N. P.; Winograd, N.; Vickerman, J. C. *Anal. Chem.* **2010**, *82*, 8291−8299.

(35) Cliff, B.; Lockyer, N.; Jungnickel, H.; Stephens, G.; Vickerman, J. C. *Rapid Commun. Mass Spectrom.* **2003**, *17*, 2163−2167.

(36) Phan, N. T. N.; Fletcher, J. S.; Sjövall, P.; Ewing, A. G. *Surf. Interface Anal.* **2014**, *46*, 123−126.

(37) Shon, H. K.; Kim, S. H.; Yoon, S.; Shin, C. Y.; Lee, T. G. *Biointerphases* **2018**, *13*, 03B411.

(38) Le, M. U. T.; Son, J. G.; Shon, H. K.; Park, J. H.; Lee, S. B.; Lee, T. G. *Biointerphases* **2018**, *13*, 03B414.

(39) Cui, W.; Li, J.; Zhang, Y.; Rong, H.; Lu, W.; Jiang, L. *Nanomedicine* **2012**, *8*, 46−53.

(40) Sheraz née Rabbani, S.; Barber, A.; Berrueta Razo, I.; Fletcher, J. S.; Lockyer, N. P.; Vickerman, J. C. *Surf. Interface Anal.* **2014**, *46*, 51−53.

(41) Inutan, E. D.; Wager-Miller, J.; Mackie, K.; Trimpin, S. *Anal. Chem.* **2012**, *84*, 9079−9084.

(42) Walworth, M. J.; ElNaggar, M. S.; Stankovich, J. J.; Witkowski, C.; Norris, J. L.; Van Berkel, G. J. *Rapid Commun. Mass Spectrom.* **2011**, *25*, 2389−2396.

(43) Poulson, B. G.; Szczepski, K.; Lachowicz, J. I.; Jaremko, L.; Emwas, A.-H.; Jaremko, M. *RSC Adv.* **2020**, *10*, 215−227.